Plant, Cell & Environment

*Plant, Cell and Environment* (2010) **33**, 431–443 doi: 10.1111/j.1365-3040.2009.02094.x

# Single-vessel flow measurements indicate scalariform perforation plates confer higher flow resistance than previously estimated

MAIRGARETH A. CHRISTMAN & JOHN S. SPERRY

*Department of Biology, University of Utah, 257 South 1400 East, Salt Lake City, UT 84112, USA*

## ABSTRACT

**During vessel evolution in angiosperms, scalariform perforation plates with many slit-like openings transformed into simple plates with a single circular opening. The transition is hypothesized to have resulted from selection for decreased hydraulic resistance. Previously, additional resistivity of scalariform plates was estimated to be small – generally 10% or less above lumen resistivity – based on numerical and physical models. Here, using the single-vessel technique, we directly measured the hydraulic resistance of individual xylem vessels. The resistivity of simple-plated lumens was not significantly different from the Hagen–Poiseuille (HP) prediction (+6 ± 3.3% mean deviation). In the 13 scalariform-plated species measured, plate resistivity averaged 99 ± 13.7% higher than HP lumen resistivity. Scalariform species also showed higher resistivity than simple species at the whole vessel (+340%) and sapwood (+580%) levels. The strongest predictor of scalariform plate resistance was vessel diameter ($r^2 = 0.84$), followed by plate angle ($r^2 = 0.60$). An equation based on laminar flow through periodic slits predicted single-vessel measurements reasonably well ($r^2 = 0.79$) and indicated that Baileyan trends in scalariform plate evolution maintain an approximate balance between lumen and plate resistances. In summary, we found scalariform plates of diverse morphology essentially double lumen flow resistance, impeding xylem flow much more than previously estimated.**

*Key-words*: ecological wood anatomy; hydraulic conductivity; plant water transport; vessel evolution; xylem flow resistance; xylem transport.

Abbreviations: $A$, cross-sectional lumen area; $a$, major axis of ellipse; $b$, minor axis of ellipse; $D$, vessel diameter; $h$, width of slit plus bar thickness; $k$, width of slit/$h$; $L$, length of scalariform slit opening; $L_e$, spacing between perforation plates; $L_v$, length of the vessel (=stem segment measured); $p$, perimeter of vessel lumen; $P$, pressure head; $r_L$, resistance of the lumen; $R_L$, resistivity of the lumen; $r_p$, resistance of the plate; $R_p$, resistivity of the plate; $r_{total}$, resistance of vessel and capillary tube; $r_{capillary}$, resistance of capillary tube; $r_{vessel}$, resistance of vessel; $R_v$, resistivity of the vessel; $t$, time; $V$, volume; $\mu$, viscosity of water.

*Correspondence: M. A. Christman. Fax: +1 801 581 4668; e-mail: m.christman@utah.edu*

## INTRODUCTION

Perforation plates are the junctions between single-celled vessel elements. They are considered homologous with pitted end walls between tracheids (Bailey & Tupper 1918). Vessels evolved from tracheids by the loss of the inter-tracheid pit membranes, leaving large perforations at the cell–cell connection. In angiosperm vessel evolution, the 'Baileyan trend' assumes that the ancestral perforation plate was scalariform with numerous bars and oriented at a low angle to the longitudinal axis. Such plates have obvious similarity in structure to scalariform pitting between tracheids of vesselless angiosperms. Remnants of the pit membranes even drape the slit-like openings in some species (Carlquist 1992). More derived plates exhibit fewer bars and higher angle and lack membrane remnants. In many lineages, scalariform plates evolved into simple plates with a single circular opening. Simple plate morphology continues the trend with oblique plates with pronounced rims considered ancestral to transverse plates with negligible rims (Bailey & Tupper 1918; Frost 1930; Bailey 1957; Carlquist 1975, 1992). The evolutionary trend towards simple perforation plates is supported by the fossil record which shows a much greater frequency of scalariform tree species in Cretaceous floras than at present (Wheeler & Baas 1993).

Natural selection for lower flow resistance is thought to have driven the transition to simple perforation plates. Carlquist suggested that species with scalariform plates can only be successful when conditions require low rates of water flow due to their presumed higher resistance (Carlquist 1975). Scalariform plates are not frequently observed in species in arid or tropical lowland areas, and are most abundant in tropical montane and temperate to arctic floras (Baas 1976). Species with scalariform perforation plates are often shorter in stature, shrubby and found in moist, understorey habitats (Carlquist 1975; Feild, Chatelet & Brodribb 2009). The implication is that simple plates were selected for in settings where hydraulic efficiency is highly advantageous, whereas scalariform plates persist when

maximizing water transport is of less competitive significance (Carlquist 1975; Baas & Schweingruber 1987; Feild *et al.* 2009).

But just how much do scalariform plates impede water transport? The data are minimal and conflicting. In a few studies which modelled water flow across plates using mathematical and large-scale physical models, the added resistivity presented by scalariform plates is minor – typically less than 10% of lumen resistivity (Schulte, Gibson & Nobel 1989; Schulte & Castle 1993a,b; Ellerby & Ennos 1998; Schulte 1999). In contrast, experiments on actual xylem vessels have suggested a much higher plate resistivity. Petty (1978) concluded that scalariform plates accounted for about half the total resistivity of vessel elements in birch (*Betula pubescens*). Even greater scalariform plate resistances were inferred from a comparative study of xylem transport in basal angiosperms (Sperry *et al.* 2007).

In this study, we resolve the ambiguous contribution of scalariform plates to flow resistance by measuring flow resistance of individual xylem vessels using the single vessel method (Zwieniecki, Melcher & Holbrook 2001b). The direct measurement of resistance in individual vessels avoids the many assumptions and calculations of previous numerical or experimental efforts (Petty 1978; Bolton & Robson 1988; Schulte & Castle 1993a,b; Sperry *et al.* 2007). Comparative measurements were made on species exhibiting a range of plate morphologies from simple to scalariform. To explore the link between plate structure and flow resistance, we applied an equation for laminar flow through periodic slits (Hasimoto 1958). We also determined whether flow resistance at the whole-branch level was increased by scalariform plates. Finally, we measured vulnerability to cavitation, vessel length and inter-vessel pit area per vessel, to see if these other aspects of xylem function co-varied with perforation plate type.

## MATERIALS AND METHODS

### Plant material

Five species with simple perforation plates were sampled for comparison with 13 species with scalariform plates using the single-vessel method. Additional scalariform species were sampled for whole-branch measurements. Species were selected to cover a wide range of phylogenetic affinity, vessel diameter and scalariform plate morphology. Table 1 lists the species, taxonomic order, plate type, measurement method (single vessel and whole branch) and collection site. Although our focus was on the listed angiosperm species, we also measured one *Ephedra* species, a gnetophyte with foraminate perforation plates (*Ephedra viridis*, collected in Grand County, UT, USA). Stem segments of approximately 1 cm diameter and 30 cm length were cut from trees, wrapped tightly in plastic to prevent desiccation and stored at 4 °C except during the day of travelling. Measurements were initiated after a day or two of storage and were completed as soon as possible, generally within 2 or 3 weeks of collection.

### Single-vessel technique

For single-vessel flow measurements, stems were cut under water to 0.5–2 cm lengths. A standard glass microcapillary (1 mm outer diameter, 0.58 mm inner diameter, World Precision Instruments, Inc., Sarasota, FL, USA) was pulled to create tips of varying size corresponding to vessel size in each species. The large end of the microcapillary was connected to a pressurized water source that was purified (Barnstead International, Dubuque IA, USA) and filtered (0.2 $\mu$m). Delivery pressure was measured on a gauge inserted along the tubing between the water source and the capillary tube. The hydraulic resistance of the microcapillary and tubing ($r_{capillary}$) was determined by dividing the delivery pressure by the volume flow rate of water. Volume flow rate was measured by timing the travel of a meniscus through a graduated pipette. The capillary tip was then inserted into one end of a vessel using a micromanipulator. Lengths of stem and microcapillary were measured individually prior to insertion and compared with total length of stem and microcapillary after insertion to account for insertion depth. Microcapillaries were secured to the stem with superglue (Loctite 409 and 712, Loctite Corp., Rocky Hill, CT, USA). Only vessels which did not include end walls were measured (see below). After letting the glue harden for 1–2 min, water was flushed through the vessel lumen at 130 kPa to remove air bubbles. Estimated bubble pressures for scalariform perforation plates are generally below 50 kPa (Bolton & Robson 1988). Following this, pressure was reduced to 60–80 kPa and resistance of the capillary plus vessel lumen ($r_{total}$) was measured. We used pure water instead of a KCl solution because in the absence of any vessel ends and intact pit membranes, resistivity would not be influenced by ionic strength or composition of the measuring solution. Although pit membrane remnants have been observed in some of the species (Table 2), ionic effects were assumed to be unlikely because remnant openings are much larger than in intact membranes.

The resistance of the vessel lumen ($r_{vessel}$) was solved by subtracting $r_{capillary}$ from $r_{total}$ based on the equation for two resistances in series:

$$r_{total} = r_{capillary} + r_{vessel} = \frac{Pt}{V} \quad (1)$$

where $P$ is the pressure difference across lumen and capillary, and $V/t$ is the volume flow rate. The resistivity of the vessel lumen ($R_v$) was calculated by dividing $r_{vessel}$ by the vessel lumen length ($L_v$ = stem length minus capillary insertion depth).

$$R_v = \frac{r_{vessel}}{L_v} \quad (2)$$

The $R_v$ of a lumen composed of repeating vessel elements is identical to the average resistivity of an individual vessel element (lumen + one perforation plate). Element resistivity in turn is composed of a lumen resistivity ($R_L$) and a plate resistivity ($R_p$) in series, such that

**Table 1.** Study species, order and collecting locale (county, state, USA)

| Species and order | | Collection locality |
|---|---|---|
| Simple-plated, single-vessel method | | |
| *Acer grandidentatum* Nutt.(Sapindales) | | Salt Lake County, UT |
| *Cercis canadensis* L. (Fabales) | | Salt Lake County, UT |
| *Hedera helix* L. (Apiales) | | Salt Lake County, UT |
| *Magnolia acuminata* L. (Magnoliales) | | Clarke County, GA |
| *Quercus gambelii* Nutt. (Fagales) | | Salt Lake County, UT |
| Scalariform-plated, single-vessel method | Abbr. | |
| *Canella winterana* (L.) Gaertn. (Canellales)* | CW | Fairchild Tropical Garden, Miami, FL |
| *Clethra acuminata* Michx. (Ericales) | CA | Polk County, NC |
| *Cyrilla racemiflora* L. (Ericales) | CR | Alachua County, FL |
| *Davidia involucrata* Baillon (Cornales)* | DI | Berkeley Botanical Garden, Berkeley, CA |
| *Illicium floridanum* Ellis (Austrobaileyales)* | IF | Calhoun County, FL |
| *Illicium parviflorum* Michx. (Austrobaileyales)* | IP | Lake County, FL |
| *Itea virginica* L. (Saxifragales)* | IV | Polk County, NC |
| *Liquidambar styraciflua* L. (Saxifragales)* | LS | Fulton County, GA |
| *Liriodendron tulipifera* L. (Magnoliales)* | LT | Fulton County, GA |
| *Magnolia fraseri* Walt. (Magnoliales)* | MF | Polk County, NC |
| *Rhizophora mangle* L. (Malphigiales) | RP | Fairchild Tropical Garden, Miami, FL |
| *Staphylea trifolia* L. (Crossosomotales)* | ST | Rutherford County, NC |
| *Symplocos tinctoria* (L.) L'Her. (Ericales)* | SY | Alachua County, FL |
| Scalariform-plated, whole-branch method | | |
| *Betula occidentalis* Hook. (Fagales) | | Salt Lake County, UT |
| *Clethra alnifolia* L. (Ericales) | | Clarke County, GA |
| *Cornus sericea* L. (Cornales) | | Salt Lake County, UT |
| *Diervilla sessilifolia* Buckley (Dipsicales) | | Haywood County, NC |
| *Gordonia lasianthus* (L.) Ellis (Ericales) | | Lake County, FL |
| *Halesia carolina* L. (Ericales) | | Polk County, NC |
| *Hydrangea arborescens* L. (Cornales) | | Polk County, NC |
| *Ilex verticillata* (L.) A. Gray (Aquifoliales) | | Polk County, NC |
| *Kalmia latifolia* L. (Ericales) | | Clarke County, GA |
| *Nyssa sylvatica* Marsh. (Cornales) | | Polk County, NC |
| *Ribes hudsonianum* Richards. (Saxifragales) | | Salt Lake County, UT |
| *Viburnum rufidulum* Raf. (Dipsicales) | | Clarke County, GA |

Species listed alphabetically in each group. Asterisks indicate single-vessel measurement species also used for whole-branch measurements. Abbreviations are listed for species with scalariform plates measured with the single-vessel method.

$$R_v = R_L + R_p \quad (3)$$

We used the Hagen–Poiseuille (HP) equation for the resistivity through cylindrical capillaries to calculate $R_L$ from the measured vessel diameter, allowing us to determine $R_p$ from Eqn 3.

The $R_p$ in Eqn 3 is the plate resistance ($r_p$) divided by the average spacing between perforation plates ($L_e$). The $L_e$ is shorter than the vessel element length which includes the full extent of two perforation plates. Measurements of $L_e$ from macerated material taken from the same stem piece (see below) allowed us to calculate $r_p$:

$$r_p = R_p L_e \quad (4)$$

The analogous equation was used to calculate the lumen resistance of the element $r_L$ ($r_L = R_L L_e$). To quantify the additional resistance or resistivity associated with the perforation plate, we calculated the '% added resistivity' as:

$$\%\ added\ resistivity = 100 \times \frac{R_p}{R_L} = 100 \times \frac{r_p}{r_L} \quad (5)$$

which represents the plate resistivity (or resistance) as a percentage of the HP lumen resistivity (or resistance).

During measurements of open capillaries, which was when the highest flow rates were achieved, the dimensionless Reynolds number, *Re* (Vogel 1994), calculated as $Re = UD/v$, where $D$ is the diameter of the pipe, $U$ is mean fluid velocity and $v$ is the kinematic viscosity of the fluid, was approximately 0.02, indicating flow was laminar and viscosity dominated. The *Re* was even lower in the xylem vessel lumen. The typical upper range in Reynolds number for xylem vessels is 0.01–0.1 (Ellerby & Ennos 1998). Thus, we were confident that our measurements represent laminar flow conditions.

After measurement, the microcapillary was detached from the water source and a small amount of safranin

**Table 2.** Perforation plate morphology and % added resistivity for single-vessel measurements

| Species | Angle (deg) | # of openings | Slit width ($\mu$m) | Bar thick ($\mu$m) | $L_e$ ($\mu$m) | % added resistivity |
|---|---|---|---|---|---|---|
| CW | 20.2 (0.3) | 16.1 (0.6) | 5.07 (0.29) | 3.41 (0.08) | 452 (26) | 140 (38) |
| CA* | 12.7 (1.6) | 56.5 (2.6) | 2.80 (0.21) | 1.23 (0.05) | 535 (25) | 100 (11) |
| CR | 15.2 (0.8) | 44.0 (8.0) | 2.48 (0.04) | 1.49 (0.04) | 425 (25) | 80 (55) |
| DI | 7.9 (0.6) | 66.4 (2.3) | 2.58 (0.07) | 1.37 (0.05) | 583 (28) | 57 (4) |
| IF* | 5.3 (0.5) | 84.0 (6.4) | 2.84 (0.12) | 2.10 (0.01) | 648 (29) | 96 (18) |
| IP* | 10.7 (0.3) | 33.1 (1.2) | 3.16 (0.13) | 1.55 (0.07) | 530 (32) | 71 (17) |
| IV | 8.9 (0.4) | 65.0 (5.4) | 2.28 (0.09) | 1.38 (0.06) | 430 (20) | 220 (50) |
| LS | 19.2 (0.3) | 20.3 (0.6) | 4.26 (0.16) | 1.52 (0.05) | 550 (37) | 110 (41) |
| LT | 20.3 (1.4) | 6.6 (0.3) | 11.90 (0.70) | 2.60 (0.09) | 580 (40) | 130 (45) |
| MF | 23.2 (1.4) | 6.1 (0.3) | 13.80 (0.33) | 3.04 (0.10) | 438 (19) | 44 ($n = 1$) |
| RP | 24.0 (0.7) | 6.0 (0.4) | 9.06 (0.22) | 4.88 (0.29) | 422 (3) | 44 (15) |
| ST | 16.0 (1.0) | 20.6 (0.7) | 4.00 (0.24) | 1.71 (0.06) | 550 (49) | 58 (15) |
| SY | 11.4 (0.6) | 39.0 (5.1) | 2.96 (0.07) | 1.53 (0.06) | 530 (67) | 130 (69) |

Species abbreviations from Table 1; asterisks are species or genera for which pit membrane remnants have been reported (Carlquist 1992). The plate angle from the longitudinal axis, number of scalariform openings per plate, their width, bar thickness, distance between plates ($L_e$) are listed as species means (SE) from macerations. The % added resistivity is the plate resistivity as a percentage of the Hagen–Poiseuille lumen resistivity (Eqn 5). The $h$ in Eqn 12 is slit width plus bar thickness, and $k$ is slit width/$h$.

dye (0.1% w/w) was injected with a syringe into the capillary. Pressure was reduced to 10 kPa and the microcapillary was attached to the tubing until the dye was observed to pass through the other end of the stem. As soon as dye was observed at the other end, the microcapillary was reattached to the water source and the dye was flushed out of the lumen of the vessel. Finally, the microcapillary was connected to an air source to confirm that the vessel lumen was open at both ends. Air pressure was slowly raised until approximately 300 kPa, which corresponds to an opening of approximately 1 $\mu$m diameter. We used a cut-off pressure of 300 kPa to allow for air penetration through perforation plates with pit membrane remnants, as has been reported for some of our species (Table 2). Most vessels showed air passing through under 150 kPa. Vessels that did not pass air below 300 kPa were assumed to end within the segment and the measurements were not used.

Stems were sectioned to obtain the diameter of the dye-stained vessel lumen. Sections were photographed at 400 times magnification and the cross-sectional area of the stained lumen was measured with Image-Pro software (Image-Pro Plus, Media Cybernetics, Inc., Bethesda, MD, USA). Approximately 4–6 pictures were analysed per vessel. In preliminary experiments with simple-plated species, the vessel diameter was measured in one of four ways. Firstly, transverse vessel areas were measured and diameters were calculated based on an equivalent circle's diameter:

$$D = 2\sqrt{\frac{A}{\pi}} \tag{6}$$

where $A$ is the lumen area. Three additional methods of calculating vessel diameter were used following options presented in Lewis (1992). Firstly, an equation for determining the hydraulic diameter of an inscribed ellipse,

$$D = \sqrt{\frac{2a^2b^2}{a^2 + b^2}} \tag{7}$$

where $a$ and $b$ are the major and minor axes, respectively. Secondly, an abbreviated equation for hydraulic diameters of elliptical openings,

$$D = 1.4a \text{ if } b > 1.6a \text{ or } D = a \text{ if } b \leq 1.6a \tag{8}$$

and thirdly, an equation based on the ratio of transverse sectional area to wetted perimeter ($P$):

$$D = \frac{4A}{P} \tag{9}$$

Results obtained from each of these calculations were plotted against the calculated HP diameter corresponding to the lumen flow resistance for simple-plated vessels. We assumed that the best method for representing vessel diameter would be the one showing the strongest correlation with the HP diameter.

Longitudinal strands of xylem split from the measured stem were macerated to measure $L_e$, and other features of perforation plate and vessel element anatomy (Table 2). Because the safranin dye used to identify the vessel for diameter measurements was not apparent after maceration, it was not possible to identify the exact vessel elements involved in the single-vessel measurement. Plate characteristics (plate length, plate width, bar number, size of openings between bars, and bar thickness) were measured on several plates for each stem and averaged to obtain a species mean. Plate angle was calculated from the length and width of the plates. Vessel element length and spacing distance between plates ($L_e$) was also measured in these macerations. The $L_e$ corresponding to the vessel diameter of

the single-measured vessel was determined from the average ratio of $L_e$ to element diameter obtained from the macerated sample.

## Derivation of an equation for scalariform perforation plate resistance

We used the data of Ellerby & Ennos (1998) on physical models of perforation plates to calibrate an equation to predict $r_p$ from vessel structure. We started with Hasimoto's equation for resistance through periodic slits in an infinitely thin plate oriented perpendicular to the direction of flow:

$$r_p = \left[\sum\left[\frac{h^2 L}{4\pi\mu} \times \ln(\cos \pi k/2)\right]\right]^{-1} \quad (10)$$

where $h$ is slit width plus bar thickness, $L$ is slit length (from vessel diameter), $k$ is slit width/$h$ and $\mu$ is viscosity (Hasimoto 1958). The summation, which we have added to the original equation, is across each slit in the perforation plate, where $L$ was calculated for each slit based on an elliptical perforation plate shape. Equation 10 gives $r_p$ for a scalariform plate at 90° to the vessel's longitudinal axis, whereas real plates are at substantially lower angles. We derived an empirical correction factor for plate angle by comparing $r_p$ from Eqn 10 with $r_p$ measured by Ellerby & Ennos (1998; see Results).

## Whole-branch resistivity

Six stems per species (Table 1) of approximately 10 mm diameter were trimmed under water to 27.5 cm length and bark was removed from each end. Stems were then flushed with 20 mM KCl at 69 kPa to remove reversible embolism. Branch resistivity was made with the standard 'gravity' method using 20 mM KCl as a measuring solution to control for ionic effects on vessel end-wall resistance. A pressure head of approximately 4–6 kPa was used (Pockman, Sperry & O'Leary 1995; Li *et al.* 2008).

Safranin dye (0.1% w/w) was perfused through the stems following the resistivity measurement. The cross-sectional area of dye-stained xylem was measured at the centre of the branch segment. Branch resistivity multiplied by sapwood area gave the sapwood-specific resistivity. Transverse sections of the segments were also made and the number of vessels per wood area was determined on three to four radial sectors of the functional xylem. Sapwood-specific resistivity was multiplied by the number of vessels per sapwood area to give the mean vessel resistivity.

Vulnerability curves showing the percentage loss in hydraulic conductivity (PLC) versus xylem pressure were obtained for a subset of whole-branch species using either the flow centrifugation (Cochard 2002; Cochard *et al.* 2005; Li *et al.* 2008) or static centrifugation methods (Alder *et al.* 1997). Despite generally good agreement with the traditional static centrifugation or 'gravity' method (Li *et al.* 2008), the flow centrifugation method sometimes results in higher conductivities (reciprocal of resistivity) at the initial (0.25 or 0.5 MPa) spin pressures relative to the initial gravity method. When this occurred, PLC was calculated relative to the highest conductivity measured (i.e. at the 0.25 or 0.5 MPa spin pressure).

Branch conductivity of six stems per species was measured as described above. Stems were then spun in a Sorvall RC-5C centrifuge (Thermo Fisher Scientific, Waltham, MA, USA) using a custom-built rotor (Li *et al.* 2008). Conductivity was measured either during spinning (flow centrifugation) or between bouts of spinning with a gravimetric head (static centrifugation). Spin speed was increased until >95% loss of conductivity was detected. The pressure at which there was 50% loss of conductivity ($P_{50}$) and the mean cavitation pressure (MCP) were calculated from a Weibull function fit to the percent loss of conductivity data for each stem and averaged for each species.

## Additional anatomical measurements

Vessel lengths were also measured for species on which branch resistivity measurements were made. We followed the silicone injection procedure of Hacke *et al.* (2007). Six stems per species were flushed with 20 mM KCl at 69 kPa to remove reversible embolism and were injected basipetally under 50–75 kPa pressure overnight with a 10:1 silicone/hardener mix (RTV-141, Rhodia, Cranbury, NJ, USA). A fluorescent optical brightener (Ciba Uvitex OB, Ciba Specialty Chemicals, Tarrytown, NY, USA) was mixed with chloroform (1% w/w) and added to the silicone (1 drop $g^{-1}$) to enable detection of silicone-filled vessels in stem sections under fluorescent microscopy. After allowing the silicone to harden for several days, stems were sectioned at five places beginning 6 mm from the injection end and ending 8–12 cm back from the cut end. The fraction of silicone-filled vessels at each length was counted and the data were fitted with a Weibull function. The best fit was then used to estimate the vessel length distribution. A full description of the procedure and equations used is presented in Christman, Sperry & Adler (2009).

Average inter-vessel pit area and number per vessel was obtained by methods detailed in Sperry *et al.* (2007). The fraction of inter-vessel walls occupied by pits was measured on longitudinal sections. The fraction of the vessel wall area in contact with adjacent vessels was estimated from cross-sections as the fraction of total vessel perimeter contacting adjacent vessels. The two fractions (pit area per inter-vessel wall, inter-vessel wall area per vessel wall area) multiplied gave the fraction of vessel wall area occupied by inter-vessel pits. This value in turn was multiplied by the average vessel wall area to give the average area of inter-vessel pits per vessel. The average vessel wall area was computed from the mean vessel length and mean diameter, assuming a cylindrical shape.

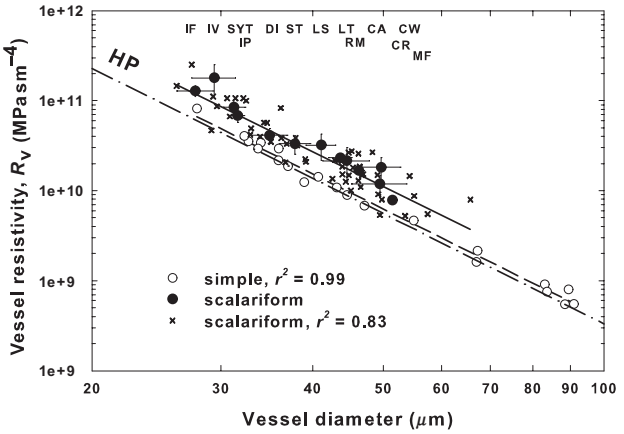


**Figure 1.** Vessel resistivity ($R_v$) by vessel diameter. Data are species averages (filled circles, abbreviations from Table 1), individual measurements for scalariform species (crosses, solid regression), and individual measurements for simple-plated species (open circles, dashed regression, species listed in Table 1). Dashed-dotted line represents the Hagen–Poiseuille (HP) equation. Species are identified by *x*-axis order with abbreviations from Table 1.

## RESULTS

### Simple-plate resistivity

Lumen resistivities measured on simple-plated species were used to predict the corresponding HP lumen diameter, which was then compared to the measured vessel diameter based on Eqns 6–9. The best relationship was with the equivalent circle diameter of Eqn 6 ($r^2 = 0.97$, data not shown), while the other three equations provided very poor fits ($r^2 = 0.36$, $r^2 = 0.12$ and $r^2 = 0.36$, respectively for Eqns 7–9). Thus we used the equivalent circle diameter to represent vessel diameter when calculating corresponding HP lumen resistivities.

Measurements on vessels with simple perforation plates from five species (Table 1) indicated a statistically negligible contribution of the perforation plate to flow resistance. Vessel resistivity decreased strongly with increasing vessel diameter ($r^2 = 0.99$) and was statistically indistinguishable from the HP lumen resistivity calculated from lumen diameter (Fig. 1, open circles versus dash-dotted HP line, slope and intercept of dashed regression not significantly different from HP line). The % added resistivity (Eqn 5) averaged 6 ± 3.3% (mean ± SE, $n = 24$ vessels) which was not different from zero ($P > 0.05$). One species, *Magnolia acuminata*, was of interest in being from a genus where many species have exclusively scalariform plates or a mixture of both plate types (InsideWood data base: http://insidewood.lib.ncsu.edu/). This species also had the highest % added resistivity at 19 ± 7.8% for $n = 3$ vessels measured. Macerations from this species indicated that the simple plates were more obliquely oriented than the other four species and with a greater rim.

### Scalariform plate resistivity

Single-vessel measurements indicated that scalariform perforation plates essentially doubled the HP resistivity of the lumen, regardless of vessel size or plate morphology (Fig. 1, crosses and species means; Table 2). The resistivity of lumens with scalariform plates decreased strongly with vessel diameter ($r^2 = 0.83$), in parallel with the decrease in HP lumen resistivity. The % added resistivity was 97 ± 10.9% on an individual vessel basis ($n = 54$, 1–6 per species) and 99 ± 13.7% (range 44–220%; Table 2) on a species mean basis. Relative to the simple-plated regression, scalariform species averaged 85 ± 12.5% added resistivity. Three single-vessel measurements showed exceptionally high resistivities relative to the others (more than three standard deviations from the mean of $n = 57$) and were excluded as outliers. *Ephedra viridis*, the vessel-bearing gymnosperm with foraminate perforation plates, showed a % increase in resistivity of 67 ± 25.5%, which was within the range for the angiosperm scalariform species (Table 2).

### Structural correlates with plate and lumen resistances

Plate and HP lumen resistivities ($R_p$, $R_L$) were converted to corresponding resistances ($r_p$, $r_L$) using the average plate spacing ($L_e$) determined from macerations (Table 2; Eqn 4). The best structural predictor of $r_p$ ($r^2 = 0.84$) and $r_L$ ($r^2 = 0.98$) was vessel diameter (Fig. 2). Both $r_p$ and $r_L$ were approximately equal and decreased together with increasing vessel diameter (Fig. 2). The next best predictor of $r_p$ was plate angle: both $r_p$ ($r^2 = 0.60$) and $r_L$ ($r^2 = 0.70$) decreased significantly with increasing plate angle (Fig. 3a). Plate angle also increased with vessel diameter ($r^2 = 0.68$,

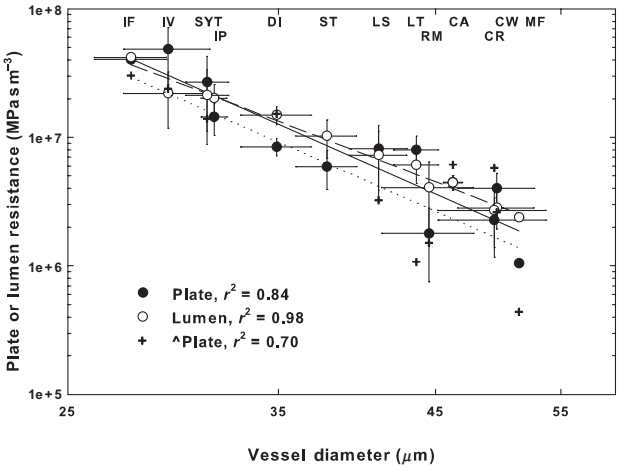


**Figure 2.** Species averages of scalariform plate (filled circles, solid regression) and vessel lumen (open circles, dashed regression) resistance by vessel diameter. Crosses and dotted regression show calculated plate resistance ($r_p$) for the species' vessel diameter and plate structure from Eqn 12. Species are identified by vessel diameter order, abbreviations from Table 1.

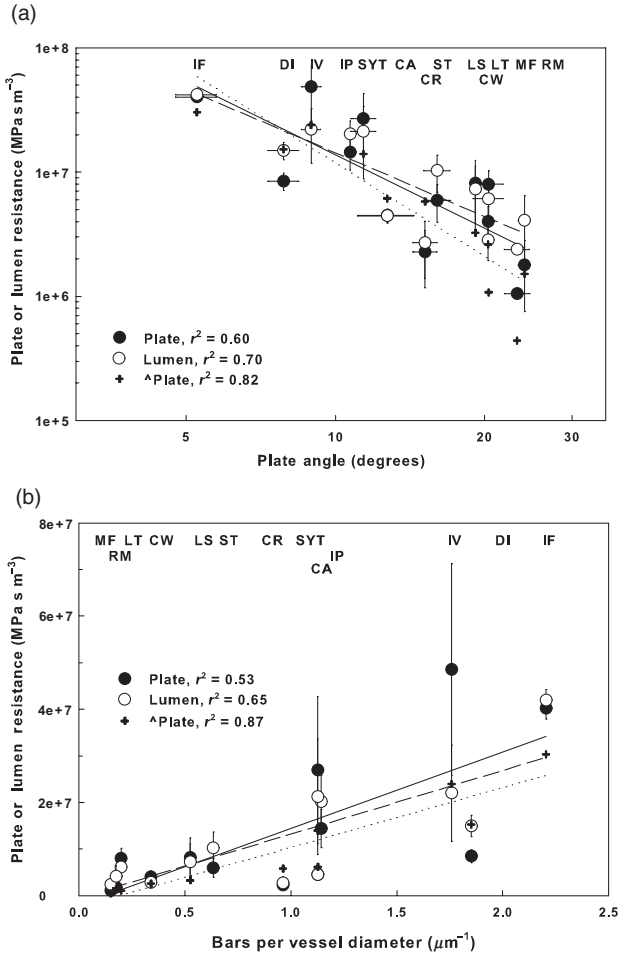


**Figure 3.** Relationship between the resistance of plate, $r_p$ (filled circles, solid regression) or lumen, $r_L$ (open circles, dotted regression) with (a) plate angle and (b) ratio of number of plate bars to vessel diameter. Crosses and dotted regression represent predicted $r_p$ from Eqn 12. Species are identified by *x*-axis order with abbreviations from Table 1.

not shown). The $r_p$ decreased significantly with increasing bar spacing (slit width), although the correlation was weak ($r^2 = 0.35$, not shown). Both angle and spacing were combined as the number of plate bars per vessel diameter. This metric is larger for low-angle plates with narrow bar spacing (presumed ancestral state), and becomes smaller for higher-angle plates with wider bar spacing (derived plates). The $r_p$ and $r_L$ both increased as the number of bars per diameter increased ($r^2 = 0.53$ and $r^2 = 0.65$, respectively; Fig. 3b), although with no greater $r^2$ than with plate angle alone. No structural parameter was found to correlate with the % added resistivity across species, which varied from a low of 44% in *Rhizophora mangle* and *Magnolia fraseri* to a high of 220% in *Itea virginica* (Table 2).

## Application of the Hasimoto's equation to scalariform plates

The 'Hasimoto resistance' (Eqn 10) was calculated for the 16 scalariform plate models measured by Ellerby & Ennos (1998). Hasimoto resistance was similar to measured resistance for the three models with 90° plates. This was expected because the Hasimoto equation assumes a 90° plate orientation. Hasimoto resistance became increasingly less than measured as plate angles became more acute. We derived an angle correction factor from the relationship between the ratio of Hasimoto to measured resistance and the sine of the plate angle ($r^2 = 0.91$, not shown):

$$C = \frac{Hasimoto\ r_p}{measured\ r_p} = 1.13 \times (\sin\theta)^{1.54} \quad (11)$$

With this correction factor, Hasimoto's equation fits Ellerby & Ennos' (1998) 16 measured resistances well ($r^2 = 0.95$; Fig. 4). The overall equation for plate conductance was thus:

$$r_p = \left[\sum\left[\frac{h^2 L}{4\pi\mu} \times \ln(\cos\pi k/2)\right]\right]^{-1} \times C^{-1} \quad (12)$$

We applied this modified Hasimoto equation to actual perforation plates using species' averages of *h*, *L*, *k* and plate angle (Table 2). The viscosity ($\mu$) was assumed to be $9.33 \times 10^{-10}$ MPa s which corresponded to the approximate temperature at which the flow measurements were made.

Calculated plate resistances (Eqn 12) were significantly correlated with single-vessel data ($r^2 = 0.79$, Fig. 5), but underestimated the measured $r_p$ by an average factor of $1.8 \pm 0.50$. Of the three species with reported pit membrane remnants (Table 2), one exceeded the calculated resistance substantially (*Illicium floridanum*) as might be expected, given that the effect of remnants is not accounted for in the equation. Just as with measured plate resistance, the calculated resistance decreased with vessel diameter (Fig. 2) and

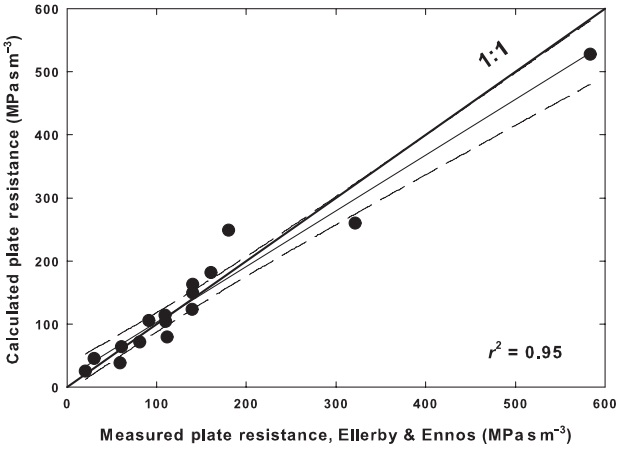


**Figure 4.** Calculated versus measured $r_p$ showing fit ($r^2 = 0.95$) of Eqn 12 to the data from Ellerby & Ennos (1998). Dashed line shows 95% confidence interval which encompassed the 1:1 line, particularly for the lower plate resistances which correspond to lower angle plates.

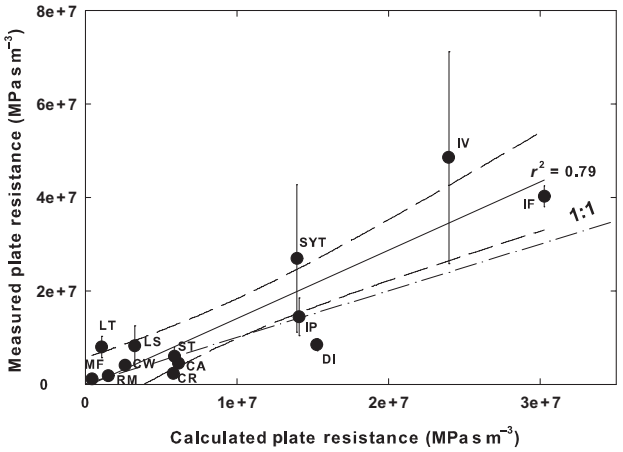


**Figure 5.** Measured $r_p$ versus calculated $r_p$ from Eqn 12 for the 13 scalariform species used in the single-vessel measurements (abbreviations from Table 1). The regression showed a generally good fit ($r^2 = 0.79$) which under-predicted resistance. Dashed-dotted line shows 1:1 relationship. Dashed line shows 95% confidence interval.

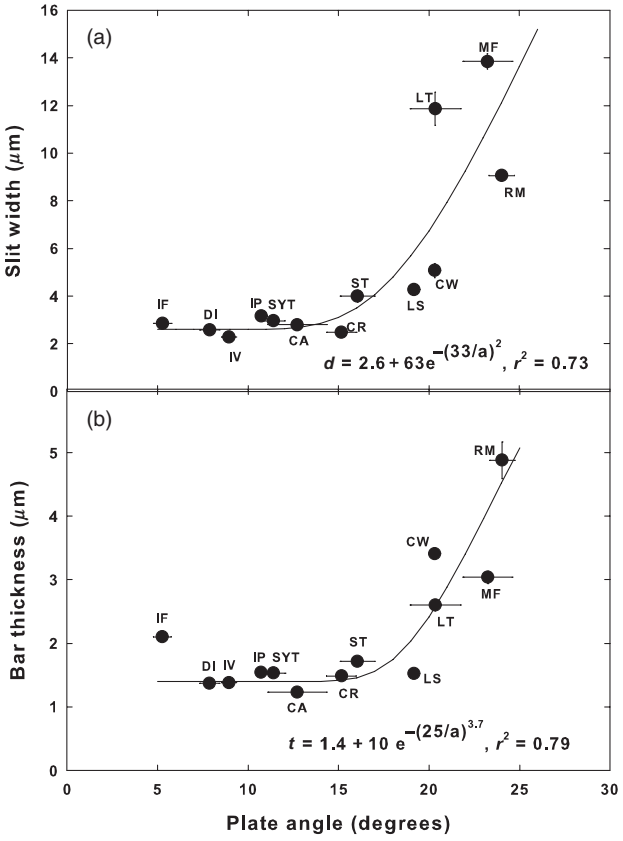


**Figure 6.** Observed relationships between plate angle and (a) slit width (distance between bars) and (b) bar thickness. Species abbreviations from Table 1. Equations are Weibull functions fit to both trends: $d$, slit width; $t$, bar thickness; $a$, plate angle.

plate angle (Fig. 3a), and increased with bars per vessel diameter (Fig. 3b). The % added resistivity of scalariform plates averaged 80 ± 14.9% for calculated values versus the 99 ± 13.7% species average from the single-vessel measurements.

Equation 12 was used to predict how trends in perforation plate morphology influenced plate resistance. We observed that bar spacing was approximately constant (2.60 ± 0.104 $\mu$m, narrowest five species, Table 2) as was bar thickness (1.4 ± 0.051 $\mu$m, thinnest five species, Table 2) for species with plate angles less than 20° (Fig. 6). This, presumably, represents ancestral anatomy. At plate angles above 20°, bars were more widely spaced and thicker (Fig. 6; Table 2), representing the derived condition. The observed increase in bar spacing with angle had the benefit of greatly enhancing the calculated decrease in plate resistance with increasing angle (Fig. 7). Plates at 25° inclination had only about 10% of the resistance for constant bar spacing with angle (Fig. 7, compare solid versus open symbols). Plate resistance would be even lower without the increase in bar thickness (calculation in Fig. 7 includes bar thickness trend in Fig. 6b).

Equation 12 predicts that $r_p$ for a fixed plate angle and bar spacing decreases with increasing vessel diameter (Fig. 8, dashed lines) because the length of the slits ($L$, in Eqn 12) increases. The fact that plate angle and bar spacing tend to increase with vessel diameter resulted in an even steeper calculated decrease in $r_p$ (Fig. 8, symbols and solid regression, same data as Fig. 2, crosses), similar to what was measured by the single-vessel method (Fig. 2, compare calculated versus measured $r_p$). The coordinated changes in plate angle, bar spacing and vessel diameter resulted in the approximate equality between plate and lumen resistances with increasing vessel diameter (Fig. 2, compare crosses with solid symbols).

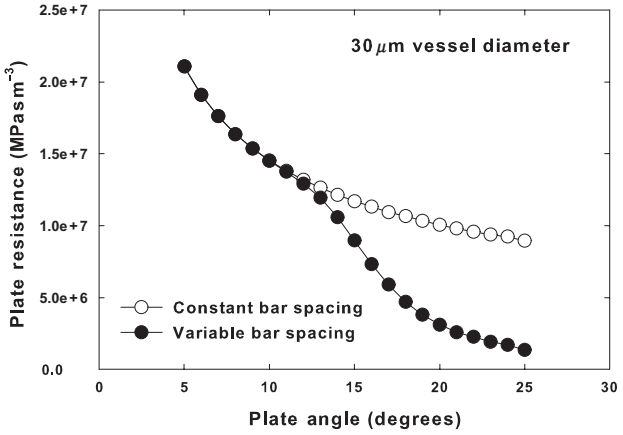


**Figure 7.** Effect of plate angle on plate resistance ($r_p$) calculated from Eqn 12. When bar spacing and thickness is constant (open circles), resistance decreases less with increasing plate angle than when bar spacing varies with plate angle as shown in Fig. 6a (closed circles). Plate resistance decreased even more when bar thickness was not allowed to increase as shown in Fig. 6b (results not shown). Calculation assumed a vessel of 30 $\mu$m diameter.

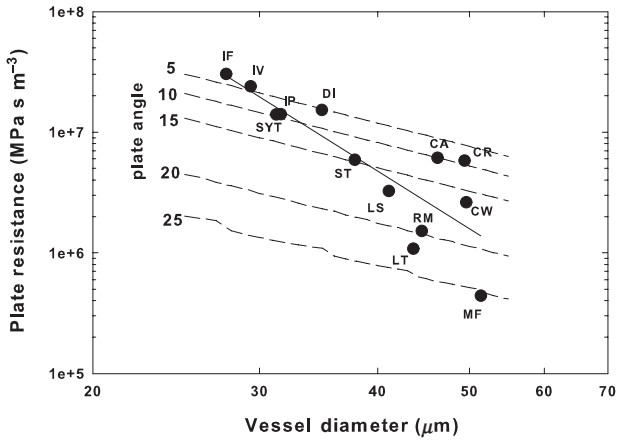


**Figure 8.** Effect of vessel diameter on plate resistance ($r_p$) based on Eqn 12. Dashed lines show the decrease in $r_p$ for plates with the same angle and bar spacing. Greater plate angles (together with Fig. 6 changes in bar configuration) lead to lower $r_p$ as also shown in Fig. 7. Coordinated changes in plate morphology with vessel diameter resulted in the strong decrease in $r_p$ with vessel diameter (species symbols, Table 1, same values plotted as crosses in Fig. 2). This decline in $r_p$ roughly matches the concomitant decline in lumen resistance (Fig. 2, compare crosses and open symbols) such that both components were approximately co-limiting across vessel size.

## Scalariform plates and whole-branch resistivity

Measured at the whole-branch level, average vessel resistivity in 22 scalariform-plated species (including 10 of 13 used for single-vessel measurements, Table 1) averaged 340 ± 108% greater resistivity per vessel than expected for a regression from 28 simple-plated species measured in a previous study by the same methods (Fig. 9, vessel resistivity). At the sapwood level, the scalariform-plated species

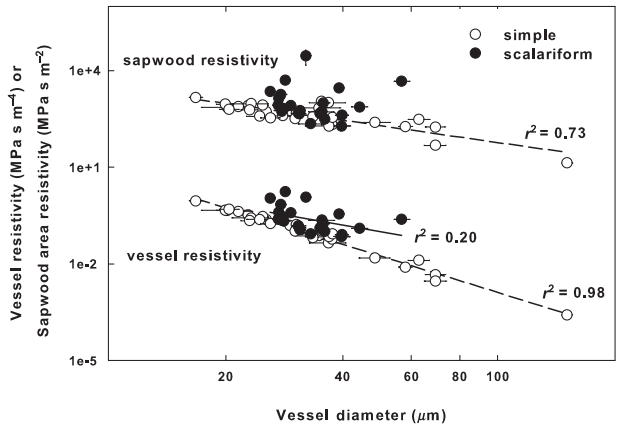


**Figure 9.** Whole-branch resistivity measurements in species with simple [open circles, dashed regression, data from Hacke *et al.* (2007)] and scalariform (closed circles, solid regression this study) perforation plates on an individual-vessel basis (vessel resistivity) or sapwood area basis (sapwood resistivity) (species abbreviations from Table 1).

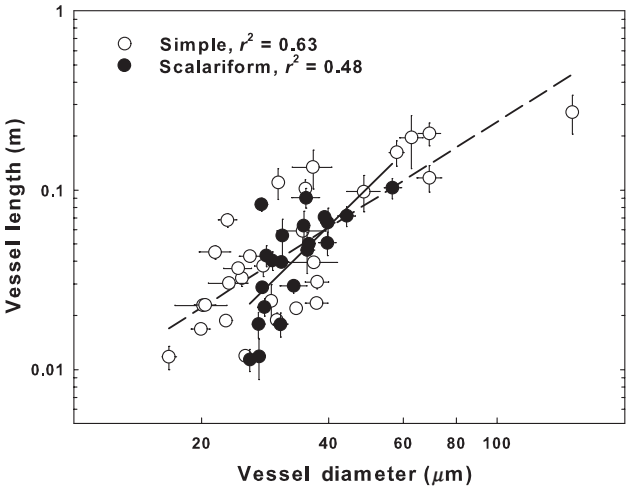


**Figure 10.** Mean vessel length versus diameter in species with simple [open symbols, dashed regression, data from Hacke *et al.* (2007)] and scalariform (closed symbols, solid line) perforation plates.

averaged 580 ± 328% greater sapwood area resistivity than the simple-plated regression [Fig. 9, sapwood resistivity; all simple-plated data from Hacke *et al.* (2007)]. These average percentage increases were greater, but much more variable, than what was observed in the single-vessel measurements (85 ± 12.5% increase relative to the simple-plate regression in Fig. 1). The greater increase in resistivity at the whole-vessel level could result from higher-vessel end-wall resistivity in scalariform-plated species. Greater end-wall resistivity could result from shorter vessels because end walls would be closer together. In most scalariform species, vessel length was similar for a given diameter as in simple-plated species [Fig. 10, simple-plate data from Hacke *et al.* (2007)]. However, there was a trend for scalariform species with narrower vessels to be shorter which could contribute to higher vessel resistivity.

## Vulnerability to cavitation and pit area in scalariform species

No systematic differences were found in the pit area by vulnerability relationship for the scalariform species as compared to simple-plated ones (Fig. 11). A few scalariform species (*I. floridanum*, *Clethra alnifolia*) had less pit area per MCP than usual, a trait previously associated with basal angiosperms (Sperry *et al.* 2007).

# DISCUSSION

The most noteworthy result was that scalariform plates essentially doubled the lumen resistivity: measured resistivity averaged 99 ± 13.7% of the HP value for an unobstructed lumen. In contrast, simple perforation plates contributed a statistically negligible increase in flow resistance (Fig. 1), consistent with previous single-vessel studies

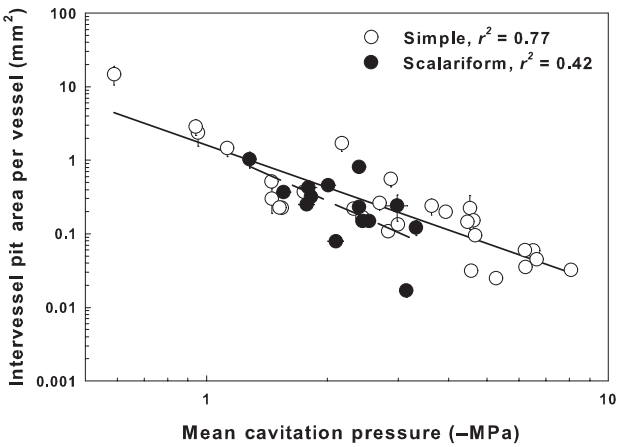


**Figure 11.** Mean cavitation pressure versus inter-vessel pit area per vessel in species with simple [open symbols, solid line, data from Hacke *et al.* (2007)] and scalariform (closed symbols, dashed line) perforation plates. Data from CW excluded because of potential artefact in cavitation pressure measurement for this long-vesseled species (Li *et al.* 2008).

(Zwieniecki *et al.* 2001b) and stem-shortening experiments (Sperry, Hacke & Pittermann 2006). Scalariform plates corresponded with even greater increases in resistivity at the vessel and sapwood levels, although there was considerable variation in these data (Fig. 9). In contrast, finite element models of flow through perforation plates of *Liriodendron tulipifera* indicated resistivity increases of only 8.7% (Schulte & Castle 1993b), and the physical models of Ellerby & Ennos (1998) all gave values below 10% (excluding their unrealistic 90° models).

Why the discrepancy between our measurements and these earlier model results? Several lines of evidence indicate that there is no major flaw in the models or error in our measurements. The modified Hasimoto equation (Eqn 12) fit *both* Ellerby & Ennos (1998)'s data and our measurements reasonably well (Figs 4 & 5), indicating generally less than 10% increases for their data and an average of 80 ± 14.9% increase for ours. In addition, Eqn 12 also indicated a 3% increase for the *L. tulipifera* plate modelled by Schulte & Castle (1993a). Bolton & Robson (1988) provide tables of plate resistance factors as a function of plate morphology from a computer model. Their tables require complex interpolation with considerable uncertainty, and are restricted to bar spacing of 5 $\mu$m or less. Nonetheless, the Bolton and Robson tables predict less than 10% for Ellerby and Ennos' and Schulte and Castle's plates, and an average increase of 122 ± 33% for our species. All of these observations indicate that the various modelling methods are at least approximately consistent with each other. The great variation in predicted plate resistance results from differences in plate morphology rather than major discrepancies between models.

The main reason for the relatively high plate resistances in our study is that our plates exhibited relatively low plate angles averaging 15.0 ± 1.69° (Table 2), and the lowest angles occurred in combination with narrow bar spacing (Fig. 6). In contrast, Ellerby & Ennos (1998) modelled plates with an average angle of 45°. Their bar spacing was either constant or increasing as plate angle decreased, neither pattern representing the trends in our data set (Fig. 6). Schulte & Castle (1993a) based their model on a plate from primary xylem of petioles which had 13 $\mu$m spacing as opposed to an average spacing of 5.2 ± 1.07 $\mu$m in our species (Table 2). Our data set represents a broader range of plate morphology than what has been modelled before, and the % added resistivity that we measured seems likely to be the rule rather than the exception.

Although previous modelling efforts all give a roughly similar % added resistivity for the same plate morphology, none are perfect in matching the single-vessel data. Equation 12 leaves 21% of the variation in the measurements unexplained (Fig. 5), and Bolton & Robson (1988)'s tables leave 28% unexplained (not shown). The models are not perfect for a number of reasons. Equation 12 was calibrated against the necessarily limited number of physical models built by Ellerby & Ennos (1998) which were tested in a lumen of constant size. Extrapolation to morphologies outside of the calibration range could increase error. Bolton & Robson (1988) provide critical assessment of the approximations inherent in their model, and mesh-size limitations can hamper finite element approaches (Schulte & Castle 1993a,b). A major missing element in any model to date is the ability to account for the presence of pit membrane remnants and other features such as anastomosing and forking of bars.

The single-vessel measurements also have sources of ambiguity. The measurements average over several plates in series and the estimated $R_p$ is an average. Variation in plate morphology within a single stem and vessel complicates a precise linkage of structure to function. Although assumed to be minor, there is a possibility in species with pit membrane remnants (see Table 2) for potential 'hydrogel' effects resulting from using pure water rather than an ionic solution for measurements (Zwieniecki, Melcher & Holbrook 2001a). Crystals or other debris could accumulate on scalariform plates under measurement conditions or potentially *in vivo* (crystals have been observed within vessels (Scurfield & Mitchell 1973; Hillis 1996), resulting in an increased flow resistance. Occlusion of plates might have been responsible for the three statistical outliers in vessel resistivity. However, all of our resistivities were obtained from flow rates that were approximately constant over time, so significant occlusion did not happen during the measurements.

The significant contribution of scalariform plates to flow resistance is consistent with previous work on the functional consequences of vessel evolution in angiosperms (Sperry *et al.* 2007). This study concluded that vessels *per se* do not improve conducting efficiency on a sapwood scale. Vessels with transitional morphology (ancestral-type perforation plates) conferred no increase in sapwood conductivity relative to vesselless wood. Furthermore, 'primitive' vessels were much less efficient per diameter than derived vessels with simple perforation plates. The inference was

made that the evolution of conducting efficiency had more to do with perforation plate evolution than the origin of vessels themselves. We included some of the same species in this study, all of which showed substantial % resistivity increases compared to HP lumen resistivities: *Canella winterana*, 141%; *I. floridanum*, 96%; *Illicium parviflorum*, 71% (Table 2).

Perhaps, the second most important result, after the magnitude of perforation plate resistance, was that despite the wide range of plate morphology that we sampled (Fig. 6; Table 2), the plate resistance remained approximately equal to vessel element lumen resistance (Fig. 2). Corollary to this result was the very strong negative correlation between plate resistance and vessel diameter (Figs 1 & 2). There was no evidence that the Baileyan trend for larger plate angle and wider bar spacing in derived plates (Fig. 6) corresponded to a decrease in % added resistivity. Plates with relatively derived morphologies had % added resistivities similar to the plates of more ancestral structure cited in the previous paragraph: for example, *Liquidambar styraciflua*, 112%; *L. tulipifera*, 131%; *Staphylea trifolia*, 57% (Table 2). We found no correlation between the % added resistivity and any aspect of plate morphology. Instead, the Baileyan trend in plate morphology maintained an approximate balance between lumen and plate resistance as vessels increased in size (Figs 2 & 8). Had there been no reduction in plate angle and increase in bar spacing with vessel size, plate resistance would not have decreased with vessel size as much as lumen resistance (Figs 7 & 8). Without the co-adjustment of plate morphology with vessel size, plate resistance would negate the advantage of wider vessels.

Our taxon sampling, although much more extensive than any previous study, is still small, and it remains to be seen how general the observed balance between plate and lumen resistances is. It was notable that the gymnosperm *E. viridis* with very different (foraminate) plate morphology exhibited a similar % added resistivity as our broader angiosperm sample (67%). It seems likely that in the very last stages of the transition between scalariform and simple plates there would have to be a drop in % added resistivity towards a near-zero value of highly derived simple plates (90° angle with negligible rims). Suggestive on this point is the comparison between the two *Magnolia* species. *Magnolia fraseri* with scalariform plates had among the lowest % added resistivity of the scalariform species at just over 44%, and *M. acuminata* with simple plates of 'primitive' morphology had the highest % added resistivity of the simple-plated species at 19%. Hypothetically, a greater sampling of species like these with derived scalariform plate morphology on the one hand and 'primitive' simple plate morphology on the other might show a continuum in % added resistivity, bridging the two apparent end points represented in our data set.

The significant resistance contributed by scalariform plates implies that a major increase in transport capacity accompanied the evolution of simple perforation plates. Previous work indicates that eudicot vessels with simple perforation plates have approximately 50% of their flow resistance in the inter-vessel end walls and 50% in their lumen (Sperry *et al.* 2006). Our results show that the lumen resistance is doubled in the presence of scalariform plates. Therefore, if all else is equal, eliminating scalariform plates would result in a 33% decrease in whole-vessel flow resistance. Our whole-branch data (Fig. 9) indicate an even larger decrease of 70% on average, meaning all else is not equal. The elimination of scalariform plates may have been accompanied by a reduction in the percentage of vessel flow resistance contributed by end walls. This would make evolutionary sense given that selective pressure for greater transport capacity would be acting on all aspects of vessel morphology, not just the perforation plate.

Although we did not analyse end-wall resistances, the tendency for at least some simple-plated species to have longer vessels for their diameter (Fig. 10) would place the end walls further apart and reduce their influence on whole-vessel resistance. Increasing the extent of inter-vessel pits and minimizing pit resistance would likewise reduce the impact of end walls. If changes in pit properties did accompany the transition in plate morphology, it apparently did not dramatically alter the relationship between pit area per vessel and vulnerability to cavitation which was largely similar between the two plate types (Fig. 11).

If evolving simple perforation plates reduced flow resistance so much, why are scalariform plates still present in so many lineages? The simplest hypothesis is that reducing flow resistance is not equally advantageous in all circumstances. It seems obvious that plants of some growth forms and in some habits (e.g. understorey plants of nutrient-poor cloud forests) do not benefit as much from enhanced water transport as others (e.g. canopy emergents or lianas). The general distribution of scalariform-plated species, which tend to occupy cooler climates with less evaporative demand and are often of low stature, is consistent with less demand for efficient water transport (Carlquist 1975; Baas 1976; Baas & Schweingruber 1987). But there are conspicuous exceptions (*L. tulipifera*, for one, is a canopy tree of the eastern USA deciduous forest) and no rigorous analysis comparing plant hydraulic efficiency to transport demands has been done across habitats and growth forms.

An alternative hypothesis for the persistence of scalariform plates is that they have advantages in some contexts. At least three advantages have been proposed, but none have any supporting evidence:

**1** Scalariform plates could act as bubble traps to prevent the formation of large air bubbles during freezing and reduce the amount of winter embolism formation (Zimmermann 1983). However, vulnerability to freezing-induced embolism is tightly correlated with vessel diameter, and similar amounts of embolism have been observed in scalariform and simple species of similar vessel size (Ewers 1985; Davis, Sperry & Hacke 1999).
**2** Scalariform plates could increase the rate of vessel refilling by dividing the air in embolized vessels into smaller bubbles (Sperry 1986). But subsequent tests of refilling

rates between species of different plate types revealed no differences (Sperry, unpublished results).

3 Scalariform plates could help prevent implosion of the vessel lumen by negative sap pressure (Carlquist 2001). There are no data or quantitative analysis that we know of to support this hypothesis either. It is curious that we observed thicker bars in presumably more derived plates with wider bar spacing (Fig. 6). Perhaps the increase in individual bar thickness was compensating mechanically for the decrease in bar number. Thicker bars are costly for flow resistance ($k/h$ decreases in Eqn 12), so their inferred evolution from thin bars is counter to the notion that selection for reduced flow resistance is the only force driving perforation plate change.

The comparative approach across lineages is useful for evaluating structure–function relationships that are independent of phylogeny. But it would also be informative to pursue lineage-specific evolution of perforation plate type and function. Such studies would be necessary to evaluate the hypothetical congruence between the competitive advantage of transport efficiency and the evolution of simple plates. These phylogenetically controlled comparisons could also better track what must be a continuum in the reduction of flow resistance as scalariform plates transition to simple ones, along with the structural correlates. The single-vessel method (Zwieniecki *et al.* 2001b) is a promising tool for pursuing such questions of perforation plate function and evolution, along with continued efforts to improve the modelling of flow through these interesting structures.

## ACKNOWLEDGMENTS

We thank Brendan Choat of the Australian National University for teaching M.A.C. the single-vessel technique. Darryl Kropf of the University of Utah generously loaned us his micro-manipulator. Holly Forbes (University of California Botanical Garden, Berkeley, CA, USA), Mary Collins (Fairchild Tropical Garden in Miami, FL, USA) and the staff of the State Botanical Garden of Georgia, Athens assisted with plant collection. David Clarke, University of North Carolina Asheville, provided North Carolina plant localities. Taylor Feild of the University of Tennessee provided useful advice on taxon sampling and manuscript editing. Most of all we thank Reid Persing and University of Utah undergraduates Ryan Edel and Spencer Crook for their long hours at the microscope making measurements. Financial support was obtained from NSF-IBN-0743148 to JSS.

## REFERENCES

Alder N., Pockman W., Sperry J. & Nuismer S. (1997) Use of centrifugal force in the study of xylem cavitation. *Journal of Experimental Botany* **48,** 665–674.

Baas P. (1976) Some functional and adaptive aspects of vessel member morphology. In *Wood Structure in Biological and Technological Research* (eds P. Baas, A. Bolton & D. Catling) pp. 157–181. Leiden University Press, Leiden, the Netherlands.

Baas P. & Schweingruber F. (1987) Ecological trends in the wood anatomy of trees, shrubs and climbers from Europe. *Bulletin of the International Association of Wood Anatomists* **8,** 245–274.

Bailey I. (1957) Additional notes on the vesselless dicotyledon, *Amborella trichopoda* Baill. *Journal of the Arnold Arboretum* **38,** 374–378.

Bailey I. & Tupper W. (1918) Size variation in tracheary cells. I. A comparison between the secondary xylems of vascular cryptograms, gymnosperms, and angiosperms. *Proceedings of the American Arts and Sciences Society* **54,** 149–204.

Bolton A. & Robson D. (1988) The effect of vessel element structure on element conductivity. *Trees-Structure and Function* **2,** 25–31.

Carlquist S. (1975) *Ecological Strategies of Xylem Evolution*. University of California Press, Berkeley, CA, USA.

Carlquist S. (1992) Pit membrane remnants in perforation plates of primitive dicotyledons and their significance. *American Journal of Botany* **79,** 660–672.

Carlquist S. (2001) *Comparative Wood Anatomy: Systematic, Ecological and Evolutionary Aspects of Dicotyledon Wood*, 2nd edn. Springer-Verlag, Berlin, Germany.

Christman M., Sperry J. & Adler F. (2009) Testing the 'rare pit' hypothesis for xylem cavitation resistance in three species of Acer. *New Phytologist* **182,** 664–674.

Cochard H. (2002) A technique for measuring xylem hydraulic conductance under high negative pressures. *Plant, Cell & Environment* **25,** 815–819.

Cochard H., Damour G., Bodet C., Tharwat I., Poirier M. & Ameglio T. (2005) Evaluation of a new centrifuge technique for rapid generation of xylem vulnerability curves. *Physiologia Plantarum* **124,** 410–418.

Davis S., Sperry J. & Hacke U. (1999) The relationship between xylem conduit diameter and cavitation caused by freezing. *American Journal of Botany* **86**, 1367–1372.

Ellerby D. & Ennos A. (1998) Resistances to fluid flow of model xylem vessels with simple and scalariform perforation plates. *Journal of Experimental Botany* **49,** 979–985.

Ewers F. (1985) Xylem structure and water conduction in conifer trees, dicot trees, and lianas. *IAWA Bulletin* **6,** 309–317.

Feild T., Chatelet D. & Brodribb T. (2009) Ancestral xerophobia: a hypothesis on the whole plant ecophysiology of early angiosperms. *Geobiology* **7,** 237–264.

Frost F. (1930) Specialization in secondary xylem of dicotyledons. I. Origin of vessel. *Botanical Gazette* **89,** 67–94.

Hacke U., Sperry J., Feild T., Sano Y., Sikkema E. & Pittermann J. (2007) Water transport in vesselless angiosperms: conducting efficiency and cavitation safety. *International Journal of Plant Science* **168,** 1113–1126.

Hasimoto H. (1958) On the flow of a viscous fluid past a thin screen at small Reynold numbers. *Journal of the Physical Society of Japan* **13,** 633–639.

Hillis W. (1996) Formation of robinetin crystals in vessels of Intsia species. *IAWA Bulletin* **17,** 405–419.

Lewis A. (1992) Measuring the hydraulic diameter of a pore or conduit. *American Journal of Botany* **79,** 1158–1161.

Li Y., Sperry J., Taneda H., Bush S. & Hacke U. (2008) Evaluation of centrifugal methods for measuring xylem cavitation in conifers, diffuse- and ring-porous angiosperms. *New Phytologist* **177,** 558–568.

Petty J. (1978) Fluid flow through the vessels of birch wood. *Journal of Experimental Botany* **29,** 1463–1469.

Pockman W., Sperry J. & O'Leary J. (1995) Sustained and significant negative water pressure in xylem. *Nature* **378,** 715–716.

Schulte P.J. (1999) Water flow though a 20-pore perforation plate in

vessels of *Liquidambar styraciflua*. *Journal of Experimental Botany* **50,** 1179–1187.

Schulte P.J. & Castle A.L. (1993a) Water flow through vessel perforation plates – a fluid mechanical approach. *Journal of Experimental Botany* **44,** 1135–1142.

Schulte P.J. & Castle A.L. (1993b) Water flow through vessel perforation plates – the effects of plate angle and thickness for *Liriodendron tulipifera*. *Journal of Experimental Botany* **44,** 1143–1148.

Schulte P.J., Gibson A.C. & Nobel P.S. (1989) Water flow in vessels with simple or compound perforation plates. *Annals of Botany* **64**, 171–178.

Scurfield G. & Mitchell A. (1973) Crystals in woody stems. *Botanical Journal of the Linnean Society* **66,** 277–289.

Sperry J. (1986) Relationship of xylem embolism to xylem pressure potential, stomatal closure, and shoot morphology in the palm *Rhapis excelsa*. *Plant Physiology* **80**, 110–116.

Sperry J., Hacke U. & Pittermann J. (2006) Size and function in conifer tracheids and angiosperm vessels. *American Journal of Botany* **93,** 1490–1500.

Sperry J.S., Hacke U.G., Feild T.S., Sano Y. & Sikkema E.H. (2007) Hydraulic consequences of vessel evolution in angiosperms. *International Journal of Plant Sciences* **168,** 1127–1139.

Vogel S. (1994) *Life in Moving Fluids*, 2nd edn. Princeton University Press, Princeton, NJ, USA.

Wheeler E. & Baas P. (1993) The potentials and limitations of dicotyledonous wood anatomy for climatic reconstructions. *Paleobiology* **19,** 487–498.

Zimmermann M. (1983) *Xylem Structure and the Ascent of Sap*. Springer-Verlag, Berlin, Germany.

Zwieniecki M., Melcher P. & Holbrook N. (2001a) Hydrogel control of xylem hydraulic resistance in plants. *Science* **291,** 1059–1062.

Zwieniecki M., Melcher P.J. & Holbrook N. (2001b) Hydraulic properties of individual xylem vessels of Fraxinus americana. *Journal of Experimental Botany* **52,** 257–264.

*Received 15 September 2009; received in revised form 17 November 2009; accepted for publication 18 November 2009*